Bioconjugate Chemistry

Article

Engineering of Photosystem I Complexes with Metal-Oxide Binding Peptides for Bioelectronic Applications.

Richard F Simmerman, Tuo F Zhu, David R Baker, Lijia Wang, Sanjay R Mishra, Cynthia A Lundgren, and Barry D Bruce

Bioconjugate Chem., **Just Accepted Manuscript** • DOI: 10.1021/acs.bioconjchem.5b00374 • Publication Date (Web): 24 Aug 2015

Engineering of Photosystem I Complexes with Metal-Oxide Binding Peptides for Bioelectronic Applications.

Richard F. Simmerman[†], Tuo Zhu[†], David R. Baker[§], Lijia Wang[‡], Sanjay R. Mishra[‡], Cynthia A. Lundgren[§], Barry D. Bruce[†*]

†Department of Biochemistry and Cellular and Molecular Biology, University of Tennessee Knoxville, Knoxville TN 37919

§U.S. Army Research Laboratory, Sensors and Electron Devices Directorate, Adelphi MD 20783

‡Department of Physics, University of Memphis, Memphis TN 38152

*Corresponding Author

Photosystem I, Bioenergy, Dye-Sensitized Solar Cells

ABSTRACT: Conventional DSSCs comprise semi-conducting anodes sensitized with complex synthetic organometallic dyes, a platinum counter electrode, and a liquid electrolyte. This work focuses on replacing synthetic dyes with a naturally occurring biological pigment-protein complex known as photosystem I (PSI). Specifically, ZnO binding peptides (ZOBiP) fused PSI subunits (ZOBiP-PsaD and ZOBiP-PsaE) and TiO_2 binding peptides (TOBiP) fused ferredoxin (TOBiP-Fd) have been produced recombinantly from E. coli. The MOBiP-fused peptides have been characterized via Western blotting, circular dichroism, MALDI-TOF, and cyclic voltammetry. ZOBiP-PSI subunits have been used to replace wild-type PsaD and PsaE, and TOBiP-Fd has been chemically cross-linked to the stromal hump of PSI. These MOBiP-peptides and MOBiP-PSI complexes have been produced and incubated with various metal-oxide nanoparticles, showing an increased binding when compared to wild type PSI complexes.

INTRODUCTION: Cyanobacteria, algae, and plants harvest solar energy, via oxygenic photosynthesis in order to convert and store chemical energy [1]. Two photosynthetic reaction centers, Photosystem II (PSII) and Photosystem I (PSI), residing in the thylakoid membranes of these organisms, are responsible for photo-induced charge separation events [2]. While both multi-subunit containing, membrane-bound photosystems have been incorporated into photovoltaic devices [3] and hydrogen producing devices[4-5], PSI has several key advantages for its use in bio-hybrid solar energy harvesting devices. These include: an extremely long functional life-time [6], a more negative reducing potential than PSII [7], placement of electron transfer cofactors, F_A and F_B outside of the hydrophobic bilayer, and the ability to specifically donate electrons to soluble acceptors ferredoxin (Fd) and flavodoxin [8].

Because of these advantages, the goal of this work is to enhance the surface selectivity of PSI through the use of binding peptides. However, a challenge that must be overcome with wild type PSI is that, when employed in a photovoltaic device it can adsorb to an electrode in a variety of configurations: including non-productively and even counter-productively as shown in Figure 1a. Different metal oxide binding peptides (MOBiP) identified and shown by phage display to selectively bind either ZnO [9], or TiO_2 [10] were engineered onto stromal subunits of PSI or Fd, respectively. We hypothesize that these ZnO and TiO_2 binding peptides (ZOBiPs/TOBiPs) will be able to increase binding efficiency and confer a uniform, productive directionality to the binding of PSI complexes onto these metal-oxide semiconductors (Figure 1b). The semiconductors ZnO and TiO_2 were chosen because of their relatively high abundance, stability, and lack of toxicity [11]. These metal-oxides and MOBiP-PSI complexes will eventually be used to create bio-hybrid dye sensitized solar cells (BH-DSSCs).

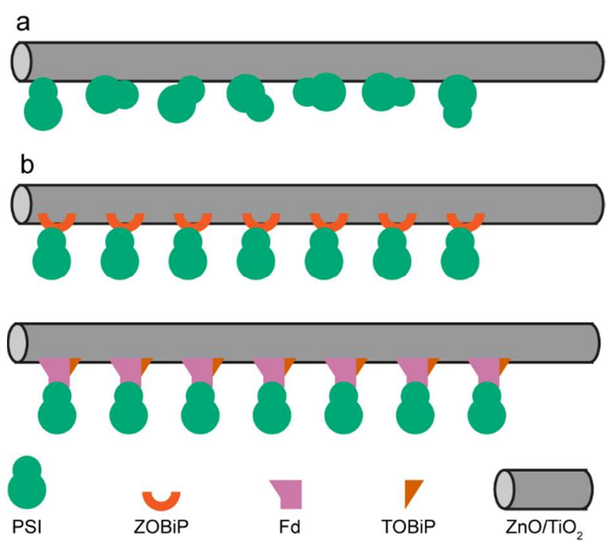

Figure 1. MOBiP-PSI Complexes Productively Bind to Metal-Oxides. (a) PSI binding to a metal-oxide semiconductor in a variety of conformations; including productive, non-productive, and counter-productive. (b) ZOBiP-PSI or TOBiP-Fd-PSI complex binding to a metal-oxide semiconductor in uniformly productive conformations.

While the efficiency of traditional DSSCs, which use ruthenium based dyes to absorb photons and inject electrons into a semiconductor (Figure 2a), has climbed to over 13% [12], there are still some limitations with these type of DSSC. These

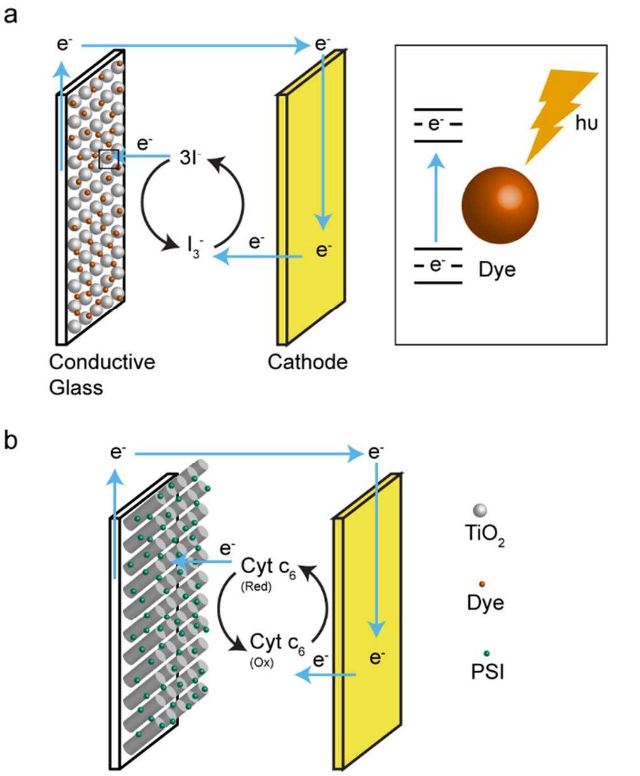

Figure 2. Traditional and Bio-Hybrid Dye Sensitized Solar Cells. (a) Traditional DSSC, with synthetic dye, TiO_2 semiconductor, conductive glass, liquid electrolyte $3I^-/I_3^-$. B) BH-DSSC, with PSI instead of a synthetic dye, and TiO_2 nanowires to increase surface area. The native electron donor to PSI, Cyt c_6 functions as the electrolyte.

include the lack of availability of the dye and platinum, which is typically used as a counter electrode, the stability of the dye, and the toxicity of the electrolyte solution [13]. It is these limitations that PSI-based BH-DSSCs (Figure 2b) can help to overcome. While most proteins are not stable for extended time, PSI has been shown to retain function in photochemical cells for months, even after the evaporation and resuspension in the electrolyte solution [6].

Although many scientists conclude that the proteinaceous basis of PSI would render it labile and limit its functional half-life. However, work in our lab and others has clearly shown that isolated PSI from cyanobacteria and plants can function to produce hydrogen or photocurrent for greater than 80 [5] and 280 days [6], respectively. Moreover, we have also made some rough calculations to show that using existing isolation methods an acre of spinach could sustainable yield enough PSI to produce very large levels of hydrogen [5] and >40 acres of PSI based solar cells [3] photocurrents. It has been estimated that using even bench-scale production methods, the materials required to fabricate the PSI based solar cells could be ~10 cents per cm^2 of active electrode area [6].

This report details bioengineering methods and reagents required to accomplish the goal of fabricating MOBiP-PSI complexes. First, recombinant ZOBiP-PSI stromal subunits PsaD and PsaE (Figure 3a) along with TOBiP-Fd (Figure 3b) were produced and purified. These modified subunits were then characterized by mass spectrometry and difference spectroscopy. Then, wild-type (WT) PsaD and PsaE incorporated in isolated PSI were replaced with ZOBiP-PsaD and ZOBiP-PsaE and TOBiP-Fd was cross-linked to WT PSI to create MOBiP-PSI complexes.

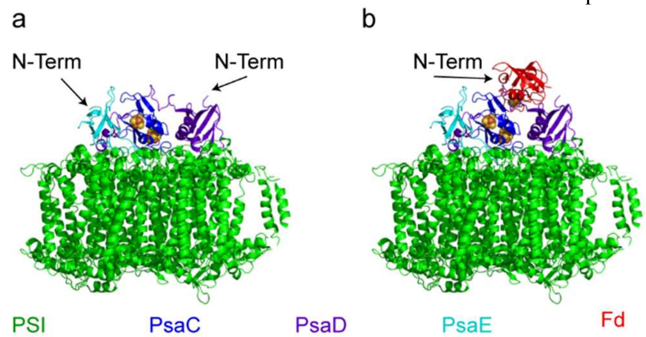

Figure 3. Accessibility of the N-termini of PsaD, PsaE and Fd. (a) PSI with the stromal hump highlighted. The [4Fe-4S] centers F_A and F_B of PsaC are shown in space-filling in yellow and orange (PDB ID 1JB0). (b) PSI-Fd (PDB ID 2CJN) model from previous work (Cashman et al. 2014).

The binding of these MOBiP-PSI complexes to their respective metal oxides was also examined and cyclic voltammatery (CV) was employed to ensure that the addition of the MOBiPs did not interfere with the abilities of the proteins to donate or accept electrons.

RESULTS AND DISCUSSION:

Engineering MOBiPs onto Photosynthetic Proteins. In the search for a mechanism that would allow PSI complexes to specifically and preferentially bind ZnO and TiO_2, peptides that had been selected for their abilities to do just that via phage-display were selected [9-10]. These MOBiPs are highly specific, for example the ZOBiP will not bind cadmium-oxide [9], but binds to ZnO very well, with 3-4 bacteria observed interacting with each ZnO particle. The high resolution crystal structure of PSI [14] allowed design of the ZOBiP-stromal subunits onto the N-termini of PsaD and PsaE to lessen the chance of interference with PSI assembly. No such crystal structure is available for the PSI-Fd complex. This was addressed in previous work using the principles of protein frustration to determine that the N-terminus of Fd is less likely to be involved in the docking of Fd-PSI [15], thus TOBiP was fused onto the N-terminus of the Fd.

Production and Purification of ZOBiP-PsaD/E and TOBiP-Fd. MOBiPs were added onto the N-termini of PSI subunits and Fd via DNA primers (Integrated DNA Technologies). The ZOBiP-PSI and TOBiP-Fd were then cloned into the pTYB2 vector (Invitrogen). This construct takes advantage of a thiol-induced cleavage to produce tagless protein. The MOBiP containing and WT proteins were recombinantly produced in *E. coli* (Figure 4a) and purified WT subunits and Fd were lyophilized and used to generate polyclonal antibodies.

Characterization of MOBiP-Peptides. After expression and purification of the ZOBiP-PSI subunits and TOBiP-Fd, the peptides were assayed to ensure that the metal-oxide binding peptides did not interfere with their structure and function. Matrix-assisted laser desorption ionization-time of flight (MALDI-TOF) mass spectrometry (MS) was used to confirm the primary structures of the WT and MOBiP proteins (Figure 4b). Circular dichroism (CD) was then performed on WT PsaD/E, ZOBiP-PsaD/E, WT-Fd, and TOBiP-Fd to confirm that the secondary structures of PsaD was not altered by the N-terminal addition of MOBiP (Figure 4c). The addition of ZOBiP to PsaE seems to confer some extra alpha helical content to the subunit. This could be due to the fact that PsaE is not complexed with the rest of PSI

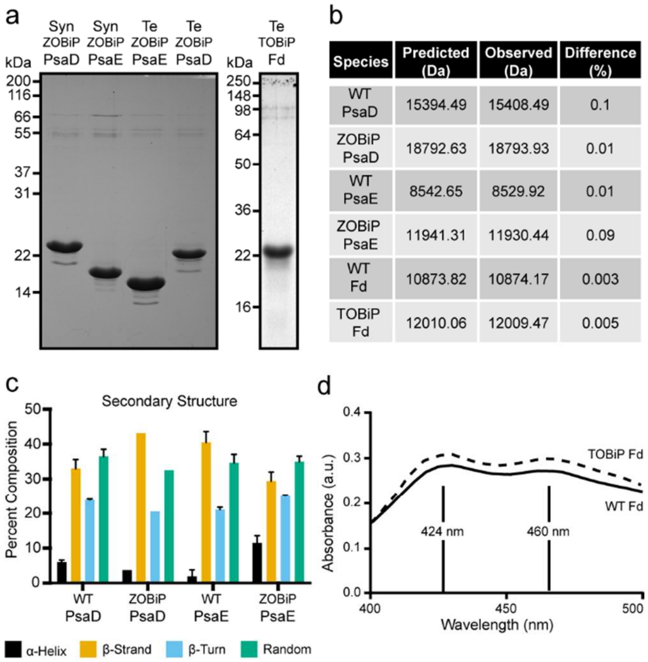

Species	Predicted (Da)	Observed (Da)	Difference (%)
WT PsaD	15394.49	15408.49	0.1
ZOBiP PsaD	18792.63	18793.93	0.01
WT PsaE	8542.65	8529.92	0.01
ZOBiP PsaE	11941.31	11930.44	0.09
WT Fd	10873.82	10874.17	0.003
TOBiP Fd	12010.06	12009.47	0.005

Figure 4. Confirmation of Recombinant MOBiP Peptides. (a) SDS-PAGE showing production and purity of ZOBiP-PsaE, ZOBiP-PsaD, and TOBiP-Fd. (b) Results from MALDI-TOF with the predicted and observed molecular weights of recombinant WT/MOBiP peptides. (c) Deconvoluted CD spectra showing the secondary structure of the WT/ZOBiP-PSI subunits. (d) Characteristic difference in absorbance spectrum of reduced-oxidized species of the WT/TOBiP Fd.

and its secondary structure is more easily perturbed as a solitary soluble peptide. The results indicated that the introduction of the MOBiPs did not perturb the secondary structures of PsaD, PsaE, or Fd. The absorbance spectra of functional Fd differs at 330 nm, 424 nm, and 460 nm, depending on the redox state of the molecule [16]. Taking the difference of the oxidized minus reduced states yields a characteristic spectrum that demonstrates Fd is functional (i.e. it can both accept and donate electrons) [16]. The addition of the TOBiP to the Fd did not alter this characteristic oxidized minus reduced spectrum, suggesting that neither the native structure nor function of the Fd was altered by the fusion of TOBiP (Figure 4d).

Optimizing Binding of MOBiP-Peptides to Metal-Oxides. After confirmation of the primary structure, secondary structure, and functionality of the MOBiP-peptides, the ability of MOBiPs to enhance binding of the fusion protein relative to wild type was investigated. Different TiO_2 binding peptides (Figure 5a), nanoparticles (NPs) (Figure 5b), buffer pH (Figure 5c) and additives (Supplemental Figure 2) were used to discover conditions that optimized binding of TOBiP-Fd. The different NPs were examined with SEM (Supplemental Figure 2). The best binding was observed in 0.1X PBS pH 7.2 with 3% (v/v) DMSO using nanospheres (NS) manufactured at the University of Memphis (Figure 5d). Experiments were performed by incubating protein with metal-oxide NPs and then separating the NPs via centrifugation. The pellets were washed and then protein was eluted from the metal-oxide by boiling with Laemmli sample buffer. This was also repeated for ZOBiP-PsaD/E, but none of the conditions tested resulted in better binding of ZOBiP-PsaD/E than WT PsaD/E to ZnO (results not shown). We hypothesized that this may not matter as the assay was attempted with soluble PsaD/E that would be far

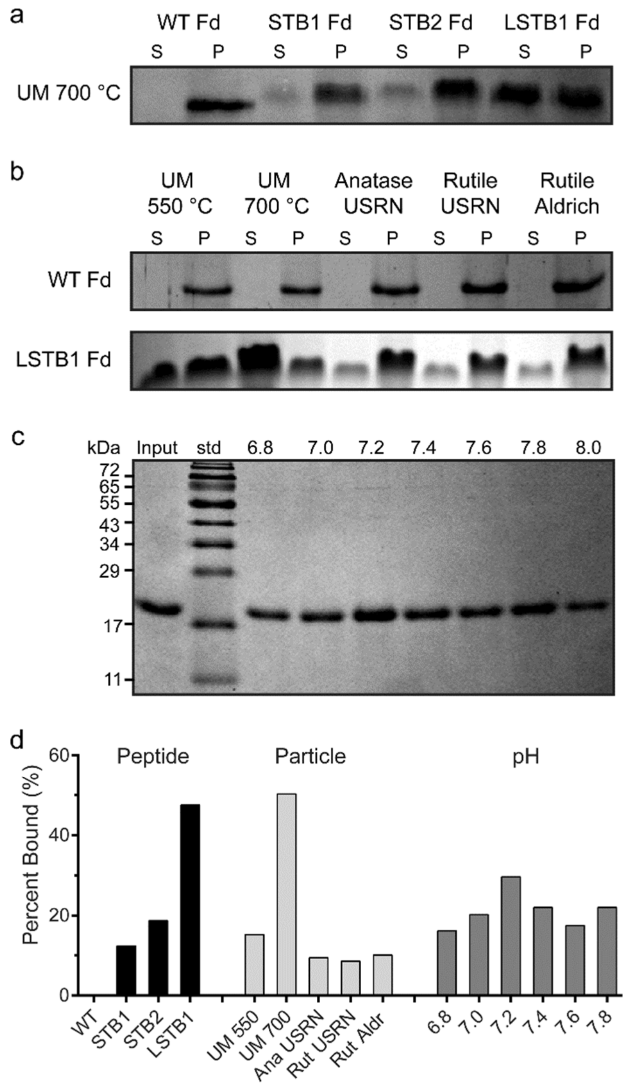

Figure 5. Optimizing Affinity of TOBiP-Fd for TiO_2. (a) SDS-PAGE with TOBiP-Fd in the supernatant [S] and pellet [P] of WT-Fd, and 3 different TOBiP-Fds incubated with TiO_2 from the University of Memphis 700 °C. (b) SDS-PAGE with TOBiP-Fd in S and P of LSTB1 TOBiP-Fd incubated with TiO_2 from the University of Memphis 700 °C, 550 °C, Anatase TiO_2 from US research nanomaterials, Rutile TiO_2 from US research nanomaterials, and Rutile TiO_2 from Aldrich. (c) SDS-PAGE of LSTB1-TOBiP-Fd in pellet with TiO_2 from the University of Memphis 700 °C in 0.1x PBS at various pH. (d) data from SDS-PAGE from A-C, quantified by ImageJ

more accessible than PsaD/E incorporated into PSI. The test was performed later with ZOBiP-PsaD/E incorporated PSI. The NSs (in particular the 700 °C calcined) from the University of Memphis were the best at TiO_2 retention. This could be explained by their smaller size, meaning their surface area to volume ratio would be the highest.

Replacing PsaD/E with ZOBiP-PsaD/E. It has previously been shown that stromal subunits PsaD and PsaE are assembled into PSI in the thylakoid membranes without the need for ATP or stromal fraction [17], and that recombinant PsaD and PsaE can replace their corresponding subunits in isolated PSI [17-18] (Figure 6a). This has been accomplished with ZOBiP- PsaE [19], however, the ZOBiP-PsaE from that work are from *M. laminosa* and incorporated into PSI from *T. elongatus*. In this present work, the

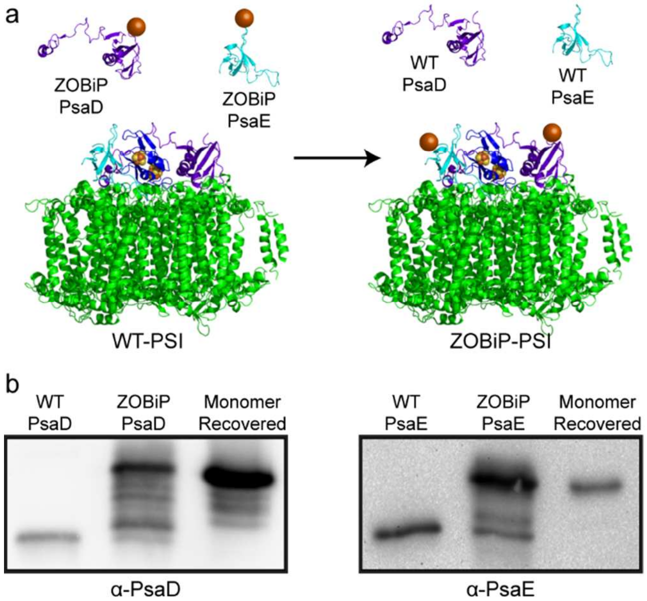

Figure 6. Replacement of WT PSI Subunits with ZOBiP-PsaD/E. (a) Replacement of PsaD/PsaE in WT PSI by incubation with ZOBiP-PsaD/E. (b) Western blot of WT PsaD/E, ZOBiP-PsaD/E, and ZOBiP-PsaD/E replaced PSI after re-recovery of PSI.

ZOBiP-PsaD and ZOBiP-PsaE are from same organism as the PSI harvested, either *T. elongatus* (T.e.) or *Synechocystis* 6803 (Syn 6803). This should allow for more complete replacement of the WT PsaD/E, and result in a more functionally active ZOBiP-PSI. This was accomplished very well (nearly 100% exchange) for Syn 6803, and nearly 50% exchange for T.e. as quantified via Western blotting (Figure 6b). Replacement reactions were performed at 20 °C, which is very close to the temperature at which Syn 6803 grows, but is roughly 30 °C colder than T.e. lives. We believe that a replacement reaction for T.e. performed at 55 °C, the temperature at which T.e. PSI naturally assembles, would result in much better replacement. All PSI complexes were recovered via ultracentrifugation over a continuous sucrose gradient.

Formation of TOBiP-Fd-PSI Complexes. ZOBiP-PSI complexes were formed via replacement of WT PsaD/E with ZOBiP-PsaD/E. Another goal of this work is to form TOBiP-Fd-PSI complexes, because Fd is the natural electron acceptor of PSI [8]. The N-terminus of Fd has been modified via addition of the TOBiP to enhance binding to TiO_2 [15]. Incorporation of Fd into a MOBiP-PSI complex could drastically decrease the chances of charge recombination by separating the electron even further from the hole left in P_{700*}. Both WT and TOBiP-Fd were chemically cross-linked to purified PSI (Figure 7). These reactions were optimized to maximize the yield of a final product that coincided with a Fd:PSI heterodimer while attempting to minimize non-specific cross-linked products (Figure 7a). All PSI complexes were recovered via ultracentrifugation over a continuous sucrose gradient. The results from the various PSI-Fd crosslinking reactions were ran on SDS-PAGE and verified by Western blotting with the antibodies that were produced earlier (Figure 7b). The results from crosslinking PSI with WT Fd were compared to the results from crosslinking PSI with TOBiP-Fd (Figure 7c). Because there was negligible difference in the Western blots (besides a small size-shift attributed to the increased size of TOBiP-Fd), the hypothesis that the TOBiP itself had no effect on the interaction between Fd and PSI was corroborated.

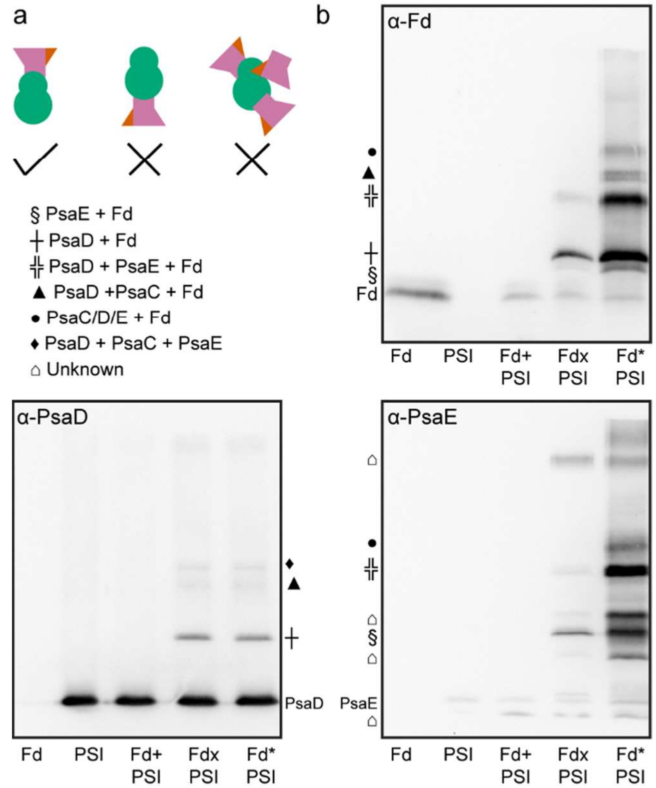

Figure 7. Crosslinking to Produce PSI-Fd Heterodimer. (a) Scheme of PSI-Fd species that is desired. (b) Western blots of the crosslinking reactions with α-PsaD, α-PsaE, and α-Fd antibodies. The FdxPSI reaction produced species consistent with a PSI-Fd heterodimer. Fd+PSI reaction was performed at 4 °C for 5 s, FdxPSI at room temperature for 5 s, and Fd*PSI at room temperature for 30 s.

Binding of PSI Complexes to Metal-Oxides is Enhanced by inclusion of MOBiPs. Because the ZOBiP did not increase binding of soluble PsaD/E compared to wild-type, the same binding assay was performed on PSI that had undergone the exchange reaction with either ZOBiP-PsaD/E or WT PsaD/E. The exchanged PSI complexes were recovered via ultracentrifugation over a continuous sucrose gradient. WT and ZOBiP PSI were then allowed to bind with ZnO NPs (US Research Nanomaterials). Samples of the unbound, washed, and bound PSI were quantitated via chlorophyll a absorbance in Figure 8a. This showed that ZOBiP-PsaD-PSI binds ~ 20% better than WT-PSI, and that ZOBiP-PsaE-PSI binds ~ 60 % better. This will be advantageous, because it means that a higher concentration of PSI may be used in BH-DSSCs that incorporate these PSI complexes. The larger increase of PSI bound by ZOBiP-PsaE-PSI may be the result of PsaE being more flexible than PsaD in the PSI complex as can be seen by the more than 60% random coil that PsaE adopts in a crystal structure [14]. This could allow PsaE to move and more effectively bridge the gap between the stromal hump of PSI and the ZnO nanoparticle. These experiments were only performed once, so although the numerical values of the gains that the MOBiPs provide are not certain, we believe that the MOBiPs will enhance binding.

PSI-Fd complexes (both WT Fd and TOBiP-Fd) generated above were also tested for their ability to bind to TiO_2. As shown in Figure 8b, the crosslinking of PSI-Fd decreases the amount of protein retained by the TiO_2 NSs when compared to PSI alone by

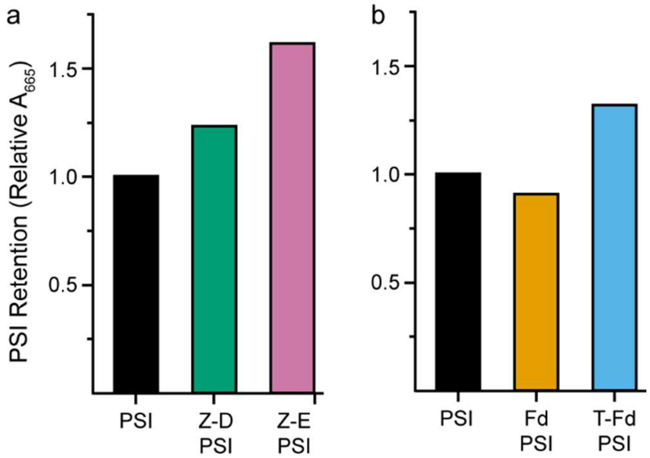

Figure 8. MOBiPs Enhance binding of PSI Complexes. (a) amount of WT-PSI, ZOBiP-PsaD-PSI, and ZOBiP-PsaE-PSI bound to NPs of ZnO. (b) amount of PSI crosslinked alone, to WT Fd, and to TOBiP-Fd bound to NSs of TiO_2. WT-PSI bound to the particle is standardized to 1.

~ 10%. However, the PSI-TOBiP-Fd binds TiO_2 45% better than PSI-Fd and 30% better than PSI alone. This means that not only can more PSI be deposited when conjugated to TOBiP-Fd, but that it is likely directionally oriented. This may allow for the creation of BH-DSSCs with the vast majority of PSI complexes in a position to productively contribute to photocurrent generation.

Redox Potentials of Fd and PSI not Altered by MOBiPs. WT-Fd and TOBiP-Fd were adsorbed to TiO_2-sintered ITO-glass slides, and WT-PSI and ZOBiP-PSI were adsorbed to ZnO-sintered ITO-glass slides. Cyclic voltammetry was used to evaluate the midpoint potentials of these species and whether the inclusion of TOBiP or ZOBiP had any effects on the electrochemical properties of the proteins. The resulting voltammograms show WT-PSI and ZOBiP-PSI (Figure 9a) along with WT-Fd and TOBiP-Fd (Figure 9b). The midpoint potentials for F_B and P_{700} of PSI (Figure 9a) and the [2Fe-2S] of Fd (Figure 9b) are highlighted on the figures and reported in Figure 9c. The voltammograms demonstrate that the addition of the MOBiPs does not alter the abilities of the proteins to donate and receive electrons, or the midpoint potential of any of the protein complexes.

In conclusion, we have incorporated a functional ZOBiP and TOBiP onto the N-termini of PsaD/E and Fd, respectively. These fusion peptides were produced recombinantly in *E. coli* (Figure 4a) and have been confirmed via MALDI-TOF (Figure 4b), CD (Figure 4c), and an altered absorbance spectrum (Figure 4d). MOBiP-PSI complexes have been assembled using ZOBiP-PsaD/E to form ZOBiP-PSI (Figure 5), and TOBiP-Fd via crosslinking to form TOBiP-Fd-PSI (Figure 6). These MOBiP-PSI complexes have been shown to have increased binding to their appropriate metal-oxide (Figure 7). Cyclic voltammetry has shown that the addition of the MOBiPs do not alter the midpoint potential of the proteins or their ability to donate and accept electrons. This will allow for increased amounts of PSI to be captured by the metal-oxide semiconductors for incorporation into BH-DSSCs. Because more protein is bound due to the MOBiP, it is reasonable to speculate that MOBiP-PSI is orientated with the MOBiP towards its corre sponding metal-oxide. The distance between the final electron acceptor in the MOBiP-PSI complex and the semiconductor may be reduced to a point that a soluble redox carrier will not be necessary to facilitate electron

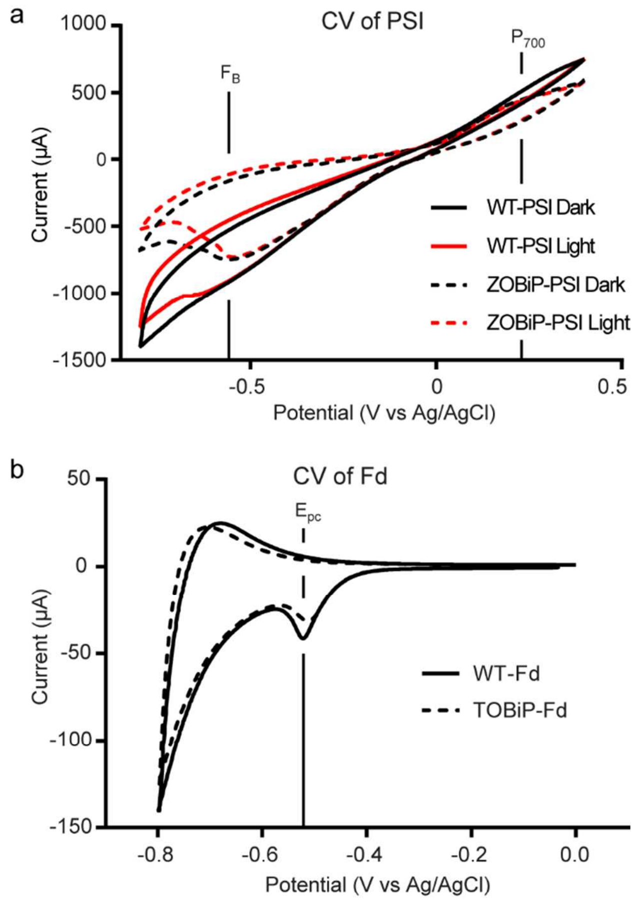

c

Species	WT P_{700}	ZOBiP P_{700}	WT F_B	ZOBiP F_B		Fd
Dark	0.27 V	0.20 V	-0.57 V	-0.54 V	WT	-0.52 V
Light	0.27 V	0.20 V	-0.59 V	-0.54 V	TOBiP	-0.51 V

Figure 9. MOBiPs do not Alter Electrochemical Properties of Proteins. (a) cyclic voltammetry of WT-PSI and ZOBiP-PSI. (b) cyclic voltammetry of WT-Fd and TOBiP-Fd. (c) midpoint potentials are unchanged by the addition of the MOBiPs.

transfer. Production and incorporation of these MOBiP-PSI complexes into electrophotochemical cells may allow for increases in photocurrent production in BH-DSSCs. This would represent a type of semiconductor-photosynthetic-protein hybrid that has been reviewed in [20]. Future work will investigate the utility of these constructs in biohybrid solar cells.

EXPERIMENTAL PROCEDURES:

General Experimental. Reagents and solvents were generally purchased from Aldrich, Gold Biotechnology, or Fisher Scientific and used as received. Dodecyl-β-D-maltopyranoside (β-DM) was purchased from Glycon Biochemicals GmbH.

Purification of PSI. Photosystem I was purified from T.e. and Syn 6803 in an identical manner, and was performed similarly to [5]. Frozen cells were resuspended in 30 mL of ice-cold lysozyme buffer (50 mM HEPES pH 8.0, 500 mM sorbitol, 10 mM $CaCl_2$, 10 mM $MgCl_2$) and homogenized in a dounce homogenizer. The chlorophyll concentration of the solution was then measured spectrophotometrically. The cells were then centrifuged at 5,000 *g* for 10 min at 4 °C. The pellet was then resuspended in ice-cold lysozyme buffer at a concentration of 1 mg/ml chlorophyll. Lysozyme was then added to a final concentration of 0.25 % (w/v) and the cells were then incubated in the dark at 37 °C for 45 min. The cells were then centrifuged at 5,000 *g* for 10 min at 4 °C. The supernatant was discarded and the cells were resuspended at 1 mg/ml chlorophyll in lysis buffer (20 mM MES pH 6.4, 10 mM CaCl2, 10 mM MgCl2, 500 mM sorbitol). Cells were then lysed via three passes through the French Press at an internal pressure of 25,000 psi. The lysate was then centrifuged at 35,000 *g* for 30 min at 4 °C. The pellet was resuspended in wash buffer (20 mM MES pH 6.4, 10 mM CaCl2, 10 mM MgCl2), homogenized, and spun again. The pellet was then resuspended at 2 mg/ml chlorophyll in wash buffer supplemented with 3 M NaBr, homogenized, diluted to 1 mg/ml chlorophyll with wash buffer, and centrifuged as above. The pellet was then resuspended at 1 mg/ml in wash buffer, homogenized, and spun again.

The protein incorporated in the washed membranes were then solubilized. The pellet was resuspended to 1.06 mg/ml chlorophyll and dodecyl-β-D-maltopyranoside (β-DM) was added to a final concentration of 0.6 % (w/v) from a 10 % (w/v) stock. The membranes were then incubated at 20 °C for 30 min with gentle shaking. The membranes were centrifuged at 35,000 *g* for 20 min and the supernatant was gently loaded on top of sucrose gradients using around 4 ml of solubilized membrane proteins per gradient. The gradients were centrifuged in a swinging bucket rotor at 100,000 *g* at rmax for at least 12 h. The lower green band was recovered, dialyzed against 1 x wash buffer, resuspended to 1 mg/ml chlorophyll and stored at -20 °C indefinitely.

Generation of WT PsaD & PsaE Primers introducing an NdeI (CAT ATG) restriction site 5' and an XmaI (CCC GGG) restriction site 3' onto psaD and psaE from Syn 6803 and T.e. were designed. Primers were synthesized by Integrated DNA Technologies, received as a lyophilized powder, and resuspended to 50 μM in ddH_2O. This constituted a 5x stock, which was aliquoted and kept frozen at -20 °C. Working stocks of primers were made by diluting the 5x stocks to 10 μM to keep the 5x stocks from contamination. PCR was performed with high fidelity ExTaq DNA polymerase (Takara Bio Inc.). PCR was performed in a Mastercycler Gradient Cycler (Eppendorf).

The PCR product was run on a 0.8 % agarose gel and purified using the Wizard SV Gel and PCR Clean-Up System (Promega). Purified PCR product was then ligated into the pGEM-T Easy vector (Promega). The product of the ligation was transformed into *E. coli* GC5 competent cells (Genesee Scientific) and spread onto 1.5 % Luria broth (LB) agar plates containing 150 μg/ml ampicillin.

Colony PCR products were run on a 0.8 % agarose gel and visually inspected to confirm that an insertion corresponding with the desired product occurred. A positive colony was sequence verified and grown overnight in LB with 150 μg/ml ampicillin. A mini-prep (Qiagen) was performed to isolate the pGEM-T Easy PSI-Subunit plasmid. DNA was quantified using A_{280} measure on a NanoDrop 3000 spectrophotometer (Thermo Scientific), aliquoted, and stored at -20 °C.

The pGEM-T Easy PSI Subunit vectors along with the pTYB2 vector (New England Biolabs) were digested with NdeI and XmaI for 90 min at 37 °C, and enzymes were heat-killed at 65 °C for 20 min. The digested pTYB2 vector was incubated with 1 μL of calf-intestine alkaline phosphatase (CIAP, Promega) for 1 h at 37 °C to remove phosphate overhangs, inhibiting self-ligation. Digested PSI-Subunit and CIAP-treated pTYB2 were run on a 0.8 % agarose gel and purified using the Wizard SV Gel and PCR Clean-Up System. The purified insert and vector were ligated for 2 h at 25 °C. The ligation products were transformed into GC5 competent cells and plated onto 1.5 % LB agar plates with 150 μg/ml ampicillin. A positive colony was selected and grown overnight at 37 °C with shaking at 225 rpm in LB with 150 μg/ml ampicillin, and a mini-prep was performed to isolate the plasmid DNA. The plasmids were quantified, aliquoted, and frozen.

Introduction of ZOBiP onto PSI Subunits The ZOBiP (zinc-oxide binding peptide) is a 25 residue peptide (Kjaergaard et al., 2000) with a 3-Glycine linker that is introduced onto the N-terminus of PsaD and PsaE. Primers coding for expression of this peptide were ordered with an NdeI cleavage site 5' and a NotI cleavage site 3'. Because of the reduction of price, 4 shorter primers with overlaps instead of 2 were purchased. Primers introducing a NotI site 5' of the PsaD/PsaE start codons were designed and purchased. This allowed us to make NdeI-NotI-PSI subunit-XmaI DNA via PCR. These were produced and ligated into pGEM-T Easy for 2 h at room temperature. The 4 primers making the ZOBiP were resuspended to 1 mM with 1 x TE buffer. Five μL of each ZOBiP primer was mixed and incubated at 95 °C 2 min, (room temp 5 min, 65 °C 3 min) 3 times and ligated into the pGEM-NdeI-NotI-PSI Subunit-XmaI vectors that were double digested with NdeI and NotI for 2 h at room temperature. Two μL of these reactions were transformed into competent GC10 *E. coli* cells and plated on 1.5 % LB agar plates with 100 μL/mg ampicillin. Insertion was verified via colony PCR.

Production of Antibodies. Polyclonal antibodies against recombinant Te-PsaD, Syn-PsaE, Te-PsaE, and Te-Fd were generated in rabbits by Agrisera Inc. from lyophilized protein purified. Two rabbits were used to generate antibodies for each antigen, and the final bleed was compared to the serum isolated from the rabbits before they were injected with the antigen to determine which antibody was most suitable for use.

Circular Dichroism Spectroscopy. The secondary structure of the PSI subunits, with and without ZOBiP, was investigated using an Aviv Series 202 circular dichroism (CD) spectrophotometer (Aviv Instruments). All purified subunits were brought to a concentration of 10 μM and extensively dialyzed into 1 x CD buffer (10 mM potassium phosphate pH 7.0, 50 mM Na2SO4). CD spectra for Syn PsaD, Syn PsaE, Syn ZOBiP-PsaD, Syn ZOBiP-PsaE, T.e. PsaD, T.e. PsaE, T.e. ZOBiP-PsaD, and T.e. ZOBiP-PsaE were generated at 25 °C from 285 to 185 nm with sampling at 1 nm intervals for 5 s. For each subunit, 3 independent scans were averaged, corrected for buffer contribution (also the average of 3 scans), smoothed, and converted to molar ellipticity using the Aviv software, version 3.37 MX. Deconvolution was performed using the CDPro software with IBase37, a reference set of 37 soluble proteins [21], to determine the probably secondary structures of the PSI subunits. CDPro uses three algorithms to deconvolute measured secondary structure: Self-Consistant method for CD analysis, version 3 (Selcon3 [22]), Contin/LL [23], and CDSSTR [24].

MALDI-TOF of PSI Subunits. Wild-type and ZOBiP-containing PsaD/E were analyzed by matrix-assisted laser desorption ionization-time of flight (MALDI-TOF) mass spectrometry (MS) to assess purity, size, and correct cleavage of the intein. MALDI-TOF MS was performed using a Bruker Daltonics Microflex ™ mass spectrometer, with β-chain insulin, ubiquitin I, cytochrome C, and β-chain myoglobin (Bruker Daltonics) used as external mass standards for calibration against all subunits produced. Lyophilized standards were resuspended to a final concentration of 50 μM in 10 μL of 50 % (v/v) acetonitrile with 0.1 % (v/v) trifluoroacetic acid. The PSI subunits and standards were mixed with 10 μL of 60 % (v/v) CHCA (α-cyano-4-hydroxycinnamic acid, Sigma-Aldrich) with 1 % (v/v) nitrocellulose. Plates were spotted with 1 μL of the mixture and incubated at room temperature overnight in a vacuum desiccator. Spectra were acquired in a positive ion mode with reflection, using 300 nitrogen laser pulses/spectrum. The resulting mass/charge data were analyzed using the FindPept program, which is freely accessible on the web at http://ca.expasy.ort/tools/findpept.html.

Western Blotting. Immobilon PVDF membrane (Millipore) was marked with a number 2 pencil and then activated in 100 % methanol for 2 min and soaked in transfer buffer (48 mM Tris, 390 mM glycine, 10 % isopropanol) for at least 5 min. Gels were run with pre-stained markers (EZ-Run Prestained, Fischer Scientific or SeeBlue, Invitrogen). Proteins were transferred from gel to the pre-soaked PVDF using a Gene transfer apparatus (Idea Scientific) at 24 V for 1.5 h at 4 °C. The blots were removed from the apparatus and incubated in 1 x TBST (25 mM Tris-HCl pH 8.0, 137 mM NaCl, 3 mM KCl, 0.1 % (v/v) Tween-20) supplemented with 3 % (w/v) NFM (non-fat milk) with gentle rocking for 1 h at room temperature with 2 buffer changes. Next, blots were incubated for 1 h with 1:25,000 primary antibody in TBST-NFM. The blots were then washed with TBST-NFM for 3 min with 2 buffer changes and then incubated with 1:50,000 secondary antibody in TBST-NFM for 1 h. The secondary antibody used was donkey-anti-rabbit horseradish peroxidase conjugated (DAR-HRP, Thermo Scientific). The blots were then washed with TBS for 15 min with 2 buffer changes. The blots were then dried by blotting on paper towels and incubated with 1 ml total volume of a 1:1 mix of HRP substrate and Luminol (Millipore) for 5 min. The signal was captured with a Chemidoc XRS (Bio-Rad) for 1.5 h taking images every 15 min. The resulting data was analyzed with Quantity One software version 4.4 (Bio-Rad) and the bands were quantitated by pixel counting.

In vitro PSI Subunit Replacement. Recombinantly produced ZOBiP-PsaD and/or ZOBiP-PsaE was exchanged with wild-type PsaD and/or PsaE of PSI isolated from Syn 6803 and T.e. in a 10 ml reaction. The final amount of wild-type PSI was 11.3 nMol, and the subunits were present at a 25-fold molar excess. Reactions took place in 1 x PSI wash buffer supplemented with 0.03 % β-DM for 2 h with gentle shaking at room temperature. After exchange, PSI was re-isolated over a sucrose gradient and exchange was verified by SDS-PAGE with Coomassie staining and/or Western blotting.

Subunit, Fd, and PSI Binding to Metal Oxides. To determine whether ZOBiP enhanced the binding of PsaD/PsaE/PSI to ZnO, a binding assay was performed using ZnO nanoparticles (10-30 nm, US Research Nanomaterials Inc.) or TiO_2 nanoparticles (from the University of Memphis). Briefly, 0.5 mg of ZnO nanoparticles was incubated with 10 μg of either: WT-PsaD, WT-PsaE, WT-PSI, ZOBiP-PsaD, ZOBiP-PsaE, ZOBiP-PsaD-PSI, or ZOBiP-PsaE in 100 μL of 0.1 x PBS (phosphate buffered saline; 10 mM Na_2HPO_4, 2 mM KH_2PO_4, 137 mM NaCl, 2.7 mM KCl). Alternatively 0.5 mg of TiO2 nanoparticles was incubated with 10 μg of either WT-Fd, STB1-Fd, STB2-Fd, or LSTB1-Fd (TOBiP-Fd) [10]. The reactions were carried out for 2 h at 4 °C with gentle agitation. The ZnO or TiO_2 was pelleted by centrifugation at 1,000 *g* for 1 m. The supernatant was collected and is marked as S in Figure 5a and 5b, and the pellet was washed twice with 100 μL of 0.1 x PBS. Finally, the ZnO or TiO_2 pellet was resuspended in 100 μL of 0.1 x PBS and boiled for 5 m. Following centrifugation, the supernatant was either mixed with 4 x LSB and SDS-PAGE was performed in the case of PSI subunits (shown as P samples in Figure 5a and 5b) or quantitated via spectrophotometry if PSI complexes were tested.

Crosslinking of PSI and Fd. PSI and Fd/TOBiP-Fd from T.e. were mixed at a 1:1 molar ratio in 0.1 x PBS with 0.03 % (w/v) β-DM. We used 3.6 nMol of each protein in each reaction with a total volume of 1 mL. The proteins were mixed and incubated on ice for 30 m, and a solution containing 125 mM EDC (1-Ethyl-3-(3-dimethylaminopropyl)carbodiimide hydrochloride; Thermo Scientific) and 250 mM NHS (N-Hydroxysuccinimide, Thermo Scientific) was pre-mixed. The EDC/NHS was added to final concentrations of 2.5 mM and 5.0 mM, respectively. The reaction was quenched with addition of 60 °C Glycine to a final concentration of 20 mM. The product of this reaction was loaded onto a sucrose gradient and PSI-complex was recovered.

Cyclic Voltammetry. With various PSI complexes or ferredoxin adsorbed to the surface of the metal-oxide ITO-glass, the ability of these complexes to donate and receive electrons was assayed by CV (cyclic voltammetry). The V.O.C. (open circuit potential) was determined for 30 s, and then the potential was set to 0 V (vs V.O.C.) and changed at a rate of 50 mV/s to -0.8 V (vs Ag/AgCl) and back to 0 V (vs Ag/AgCl). This scan was performed for 5 cycles with the sample slide in 200 mM sodium phosphate pH 6.4. The first 3 cycles were in the dark and the next 2 were illuminated with 1.4 mW/cm2 676 nm band-pass filtered light.

Synthesis of Hollow Porous TiO_2 Nanospheres. The TiO_2 nanospheres (NS) were synthesized via hydrothermal method in presence of glucose. 7.5 g of glucose and 1.5 g of $(NH_4)_2TiF_6$ were dissolved in 40 ml and 20 ml of distilled water, respectively. The two solutions were mixed by stirring for 30 min. The resulting solution was poured into Teflon coated stainless-steel autoclave (80 ml). The autoclave was placed into the furnace at 180°C for 24 hours. After the autoclave was cooled naturally to room temperature, the resultant product of semi-crystalline precipitates of TiO_2 embedded in the caramelized glucose was centrifuged for collection. The as synthesized precipitates were washed at least five times with distilled water and ethyl alcohol. The resulting precipitates were then dried at 80°C for 15 hours. The dried precipitates were calcined at either 550 °C or 700 °C for 3 hours to obtain highly crystalline and porous anatase TiO_2 nanospheres [25-26] as confirmed by x-ray diffraction and scanning electron microscope.

ASSOCIATED CONTENT

Supporting Information. Different TiO_2 nanoparticles and nanospheres observed by EM and the effects of various additives on TOBiP-Fd retention by TiO_2 is supplied as Supporting Information. "This material is available free of charge via the Internet at http://pubs.acs.org."

AUTHOR INFORMATION

Corresponding Author

* Barry D. Bruce, Department of Biochemistry and Cellular and Molecular Biology, University of Tennessee Knoxville, Knoxville TN 37919. bbruce@utk.edu

Present Addresses

†If an author's address is different than the one given in the affiliation line, this information may be included here.

Author Contributions

The manuscript was written through contributions of all Richard Simmerman, Tuo Zhu, and Barry Bruce. David Baker performed CV measurements and Lijia Wang manufactured the titanium oxide. / All authors have given approval to the final version of the manuscript.

Funding Sources

BDB and SRM acknowledge support from TN-SCORE, a multi-disciplinary research program sponsored by NSF-EPSCoR (EPS-1004083) and BDB support. RFS, TZ, and BDB acknowledge support from the UTK BCMB Department and from the Gibson Family Foundation. RFS was supported as an IGERT Fellow from the National Science Foundation IGERT program (DGE-0801470). BDB, DRB, and CAL also acknowledge support from the Directors Strategic Initiative, "Understanding Photosystem I as a Biomolecular Reactor for Energy Conversion" at the Army Research Laboratory, Adelphi, MD (ARL Contract #W911NF-11-2-0029).

ACKNOWLEDGMENT

We would like to thank Dr. John Dunlap for help with electron microscopy. We also appreciate the support and feedback provided by Ridge Carter, Khoa Nguyen, and Kristen Holbrook while conducting this research.

ABBREVIATIONS

DSSC, dye-sensitized solar cell; Fd, ferredoxin, MOBiP, metal-oxide binding peptide; PSI, photosystem I; TOBiP, titanium-oxide binding peptide; ZOBiP, zinc-oxide binding peptide.

REFERENCES

1. Blankenship, R. E., Hartman, H., 1998, The origin and evolution of oxygenic photosynthesis. *Trends Biochem Sci 23* (3), 94-7.
2. Rochaix, J. D., 2011, Regulation of photosynthetic electron transport. *Biochimica et biophysica acta 1807* (3), 375-83.
3. Nguyen, K., Bruce, B. D., 2014, Growing green electricity: Progress and strategies for use of Photosystem I for sustainable photovoltaic energy conversion. *Biochimica et biophysica acta 1837* (9), 1553-1566.
4. Kim, Y., Shin, D., Chang, W. J., Jang, H. L., Lee, C. W., Lee, H.-E., Nam, K. T., 2015, Hydrogen Evolution: Hybrid Z-Scheme Using Photosystem I and BiVO4 for Hydrogen Production (Adv. Funct. Mater. 16/2015). *Advanced Functional Materials 25* (16), 2345-2345.
5. Iwuchukwu, I. J., Vaughn, M., Myers, N., O'Neill, H., Frymier, P., Bruce, B. D., 2010, Self-organized photosynthetic nanoparticle for cell-free hydrogen production. *Nature nanotechnology 5* (1), 73-9.
6. Ciesielski, P. N., Hijazi, F. M., Scott, A. M., Faulkner, C. J., Beard, L., Emmett, K., Rosenthal, S. J., Cliffel, D., Kane Jennings, G., 2010, Photosystem I - based biohybrid photoelectrochemical cells. *Bioresource technology 101* (9), 3047-53.
7. Merchant, S., Sawaya, M. R., 2005, The light reactions: a guide to recent acquisitions for the picture gallery. *The Plant cell 17* (3), 648-63.
8. Zanetti, G., Merati, G., 1987, Interaction between photosystem I and ferredoxin. Identification by chemical cross-linking of the polypeptide which binds ferredoxin. *European journal of biochemistry / FEBS 169* (1), 143-6.
9. Kjaergaard, K., Sorensen, J. K., Schembri, M. A., Klemm, P., 2000, Sequestration of zinc oxide by fimbrial designer chelators. *Applied and environmental microbiology 66* (1), 10-4.
10. Chen, H., Su, X., Neoh, K. G., Choe, W. S., 2008, Probing the interaction between peptides and metal oxides using point mutants of a TiO2-binding peptide. *Langmuir : the ACS journal of surfaces and colloids 24* (13), 6852-7.
11. Macwan, D. P., Dave, P. N., Chaturvedi, S., 2011, A Review on Nano-TiO2 Sol-gel Type Synthesis and its Applications. *Journal of Materials Science 46* (11), 3669-3686.
12. Mathew, S., Yella, A., Gao, P., Humphry-Baker, R., Curchod, B. F., Ashari-Astani, N., Tavernelli, I., Rothlisberger, U., Nazeeruddin, M. K., Gratzel, M., 2014, Dye-sensitized solar cells with 13% efficiency achieved through the molecular engineering of porphyrin sensitizers. *Nature chemistry 6* (3), 242-7.
13. Chang, H., Hsu, C.-M., Kao, P.-K., Yang, Y.-J., Hsu, C.-C., Cheng, I. C., Chen, J.-Z., 2014, Dye-sensitized solar cells with nanoporous TiO2 photoanodes sintered by N2 and air atmospheric pressure plasma jets with/without air-quenching. *Journal of Power Sources 251* (0), 215-221.
14. Jordan, P., Fromme, P., Witt, H. T., Klukas, O., Saenger, W., Krauss, N., 2001, Three-dimensional structure of cyanobacterial photosystem I at 2.5 A resolution. *Nature 411* (6840), 909-17.
15. Cashman, D. J., Zhu, T., Simmerman, R. F., Scott, C., Bruce, B. D., Baudry, J., 2014, Molecular interactions between photosystem I and ferredoxin: an integrated energy frustration and experimental model. *Journal of molecular recognition : JMR 27* (10), 597-608.
16. Hall, D. O., Cammack, R., Rao, K. K., The plant ferredoxins and their relationship to the evolution of ferredoxins from primitive life. In *Pure and Applied Chemistry*, 1973; Vol. 34, p 553.
17. Minai, L., Fish, A., Darash-Yahana, M., Verchovsky, L., Nechushtai, R., 2001, The assembly of the PsaD subunit into the membranal photosystem I complex occurs via an exchange mechanism. *Biochemistry 40* (43), 12754-60.
18. Lushy, A., Verchovsky, L., Nechushtai, R., 2002, The stable assembly of newly synthesized PsaE into the photosystem I complex occurring via the exchange mechanism is facilitated by electrostatic interactions. *Biochemistry 41* (37), 11192-9.
19. Mershin, A., Matsumoto, K., Kaiser, L., Yu, D., Vaughn, M., Nazeeruddin, M. K., Bruce, B. D., Graetzel, M., Zhang, S., 2012, Self-assembled photosystem-I biophotovoltaics on nanostructured TiO(2)and ZnO. *Scientific reports 2*, 234.
20. Kim, Y., Shin, S. A., Lee, J., Yang, K. D., Nam, K. T., 2014, Hybrid system of semiconductor and photosynthetic protein. *Nanotechnology 25* (34), 342001.
21. Sreerama, N., Venyaminov, S. Y., Woody, R. W., 2000, Estimation of protein secondary structure from circular dichroism spectra: inclusion of denatured proteins with native proteins in the analysis. *Analytical biochemistry 287* (2), 243-51.
22. Sreerama, N., Venyaminov, S. Y., Woody, R. W., 1999, Estimation of the number of alpha-helical and beta-strand segments in proteins using circular dichroism spectroscopy. *Protein Sci 8* (2), 370-80.
23. Provencher, S. W., Glockner, J., 1981, Estimation of globular protein secondary structure from circular dichroism. *Biochemistry 20* (1), 33-7.
24. Johnson, W. C., 1999, Analyzing protein circular dichroism spectra for accurate secondary structures. *Proteins 35* (3), 307-12.
25. Wang, H. Q., Wu, Z. B., Liu, Y., 2009, A Simple Two-Step Template Approach for Preparing Carbon-Doped Mesoporous TiO2 Hollow Microspheres. *J Phys Chem C 113* (30), 13317-13324.
26. Liu, G., Yan, X. X., Chen, Z. G., Wang, X. W., Wang, L. Z., Lu, G. Q., Cheng, H. M., 2009, Synthesis of rutile-anatase core-shell structured TiO2 for photocatalysis. *J Mater Chem 19* (36), 6590-6596.

SYNOPSIS TOC